Journal of the Serbian Society for Computational Mechanics / Vol. 19 / No. 1, 2025 / pp 282-295 / review paper
(10.24874/jsscm.2025.19.01.17)

HEART MODELING, INSILICO CLINICAL TRIALS

Nenad Filipovic[1,2*] [0000-0001-9964-5615], Igor Saveljic[1,2] [0000-0002-0707-5174], Tijana Geroski[1] [0000-0003-1417-0521], Smiljana Tomasevic[1,2] [0000-0002-5614-5730], Miljan Milosevic[2,3] [0000-0003-3789-2404], Bogdan Milicevic[2,3] [0000-0002-0315-8263], Momcilo Prodanovic[2,3,4] [0000-0003-0556-1213], Srboljub Mijailovic[4] [0000-0003-2640-3548] and Milos Kojic[2] [0000-0003-2199-5847]

[1] Faculty of Engineering University of Kragujevac, Kragujevac, Serbia
[2] BioIRC Bioengineering Research and Development Center, Kragujevac, Serbia
[3] Institute for information technology, Kragujevac, University of Kragujevac
[4] FilamenTech, Inc., Newton, MA, USA
email: **fica@kg.ac.rs**
**corresponding author*

Abstract

In silico clinical trials are set to transform medicine by enabling virtual testing and simulation, which streamline the development of medical devices and pharmaceuticals while reducing costs and duration. The SILICOFCM platform offers a innovative, multi-modular approach designed to optimize overall heart function and monitor the effectiveness of pharmacological treatments, aiming to decrease dependence on animal and human trials. It employs an integrated, multidisciplinary, and multiscale methodology to analyze patient-specific data, allowing the creation of personalized models that track disease progression. By combining data from various sources and scales with advanced computational techniques, SILICOFCM maps the flow of information from genetic mutations to organ dysfunction. The platform specifically targets hypertrophic (HCM) and dilated (DCM) cardiomyopathy through coupled macro- and micro-scale simulations utilizing finite element modeling of fluid-structure interaction (FSI) and molecular interactions within cardiac cells. This enables the simulation of left ventricular mechanics and the assessment of how different drugs influence electro-mechanical processes, including changes in calcium (Ca2+) handling and kinetic parameters. The overarching goal of the STRATIFYHF project is to develop and clinically validate an innovative AI-driven Decision Support System (DSS) to predict heart failure risk, support early diagnosis, and forecast disease progression—offering a paradigm shift in heart failure management across primary and secondary care. The DSS integrates patient-centered data from existing and emerging technologies, a digital patient library, and AI-based algorithms combined with computational modeling. Through workflows dedicated to improving heart performance and evaluating pharmacological effects, SILICOFCM and STRATIFYHF are paving new pathways to accelerate drug development and clinical testing.

Keywords: cardiac cycle, finite element method, muscle mechanics, electrophysiology, cardiomyopathy

1. Introduction

Transport through biological barriers, such as vessel walls and cell or organelle membranes, is influenced by the hydraulic or diffusion coefficients of these barriers and the size of the separating surfaces between different continuum domains (Guyton et al. 1972, Katona et al. 1979, Carney et al. 2009). In the field of electrophysiology, the objective is to characterize the electrophysiological properties of various body compartments and the patterns of signal propagation (Lauer et al. 2009, Rashba et al. 2002, Piccirillo et al. 2009). The SILICOFCM project (2018-2023) modeled familial cardiomyopathy using a comprehensive array of patient-specific features, incorporating genetic, biological, pharmacologic, and clinical imaging data. A coupled model was developed that integrates multiscale modeling of a realistic sarcomeric system, patient genetic profiles, electrophysiology, accurate muscle fiber directional data, and solid-fluid interactions related to heart electrophysiology. Preliminary findings indicated that deformations in the left ventricle affect the subsequent deformation of the mitral valve and overall blood flow in the heart. Furthermore, the study assessed drug distribution within the heart and the effects of various pharmacological agents using the cardiomyopathy model, providing valuable insights into potential treatment strategies. Accurate risk stratification and early diagnosis of Heart Failure (HF) allow implementation of evidence-based prevention and treatment strategies which reduce HF morbidity and mortality and its burden on healthcare. The clinical guidelines for HF recommend the use of risk stratification models to estimate prognosis but these are limited and not implemented in clinical practice. Early diagnosis is challenging, often inaccurate as initial signs and symptoms are non-specific (STRATIFYHF 2023). In this review we present some results from SILICOFCM project related to electrocardiograph simulation and simulation of left ventricle mechanics, defining kinetic processes for different drug influences on electro-mechanics using Ca2+ and kinetic parameters.

2. Fundamental relations

2.1 Electrocardiogram ECG

An electrocardiogram (ECG) is a recording of the heart's electrical activity, captured through projections known as leads that are positioned along specific axes based on electrode placement. These leads provide a view of the heart's electrical signals from various angles across the body. The 12-Lead ECG became a standard diagnostic tool in clinical practice following the American Heart Association’s recommendation in 1954. It involves recording signals from 10 electrodes placed at designated sites as shown in Figure 1,

V1: 4th intercostal space to the right of the sternum
V2: 4th intercostal space to the left of the sternum
V3: midway between V2 and V4
V4: 5th intercostal space at the midclavicular line
V5: anterior axillary line at the same level as V4
V6: midaxillary line at the same level as V4 and V5

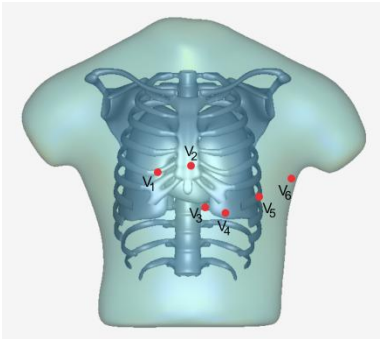

Fig. 1. Six electrodes (V1-V6) which are positioned on the chest to model the precordial leads

Numerical simulations were conducted using the fully coupled heart torso monodomain equations including detailed description of human ventricular cellular electrophysiology (Gibbons Kroeker et al 2006, Pullan et al 2005b). Myocardial and torso conductivities were based on the literature, as presented in Table I (Trudel et al 2004, Wilhelms et al 2011, Fitzhugh 1961 Nagumo 1962).

Parameter	**SAN**	**Atria**	**AVN**	**His**	**BNL**	**Purkinje**	**Ventricles**
A	-0.60	0.13	0.13	0.13	0.13	0.13	0.13
B	-0.30	0	0	0	0	0	0
c_1(AsV^{-1} m^{-3})	1000	2.6	2.6	2.6	2.6	2.6	2.6
c_2 (AsV^{-1} m^{-3})	1.0	1.0	1.0	1.0	1.0	1.0	1.0
D	0	1	1	1	1	1	1
E	0.066	0.0132	0.0132	0.005	0.0022	0.0047	0.006
A (mV)	33	140	140	140	140	140	140
B (mV)	-22	-85	-85	-85	-85	-85	-85
K	1000	1000	1000	1000	1000	1000	1000
σ ($mS{\cdot}m^{-1}$)	0.5	8	0.5	10	15	35	8

Table 1. Coefficient determined experimentally and computed by approximate expressions.

The methodology was validated using a comprehensive 3D heart model grounded in a linear elastic, orthotropic material framework derived from Holzapfel's experiments (Holzapfel, 2006). With this approach, it is possible to precisely simulate the propagation of electrical signals and the displacement field within the heart tissue. This technique has the potential to be integrated into coupled solid-fluid simulations of the entire heart, enabling accurate predictions of heartbeat dynamics across various cardiac conditions (Sovilj, 2013).

Boundary conditions on all interior boundaries Vm, which are in contact with the torso, lungs, and cardiac cavities, are zero flux; therefore, $-\mathbf{n} \cdot \mathbf{\Gamma} = 0$ where $\mathbf{n}$ is the unit outward normal vector on the boundary and $\mathbf{\Gamma}$ is the flux vector through that boundary for the intracellular voltage, equal to $\mathbf{\Gamma} = -\sigma \cdot \partial V\text{m}/\partial \mathbf{n}$. For the variable Vm, the inward flux on these boundaries is equal to the outward current density $\mathbf{J}$ from the torso/chamber volume conductor; therefore, $-\sigma \cdot \partial V\text{m}/\partial \mathbf{n} = \mathbf{n} \cdot \mathbf{J}$. (Kojic et al 2019)

In the second part, we implemented classical approaches for solving the ECG inverse problem using the epicardial potential formulation. The studied methods are the family of Tikhonov methods and L regularization based methods (Wang and Rudy 2006, Van Oosterom 1999,

2001, 2003, 2010). ECG measurement was performed in the Clinical Center Kragujevac, University of Kragujevac on a healthy volunteer.

2.2 Fluid-structure interaction

In this study, the fluid-structure interaction (FSI) algorithm for finite element (FE) simulation was initially introduced, followed by an explanation of how the FE model was integrated with muscle fiber stretch analysis. The primary actions of specific drugs were categorized into two main groups: the first group includes drugs that modulate calcium transients (Disopyramide and Digoxin), while the second group comprises drugs that alter the kinetics of contractile proteins (Mavacamten and 2-deoxy adenosine triphosphate, dATP). We quantitatively examined the effects of these drugs on pressure and volume changes within a left ventricle (LV) model tailored for patients with hypertrophic cardiomyopathy (HCM) or dilated cardiomyopathy (DCM). Additionally, results from the Risk Stratification Tool for five HCM patients were presented and compared with observations from the SILICOFCM clinical study. Finally, data on pressure, displacement, and velocity distribution, as well as pressure-volume (P-V) loops for LV HCM and LV DCM patients under baseline conditions and following drug influence, were provided (MUSICO 2023, Mijailovich et al., 2021a, 2021b; Prodanovic et al., 2022).

2.3 Fluid-solid coupling

The movement of fluid in the left ventricle can be considered as a laminar flow of the incompressible fluid, which is described using the continuity equation and Navier-Stokes equations:

$$-\mu\nabla^2 v_l + \rho\left(v_l \cdot \nabla\right)v_l + \nabla p_l = 0 \tag{1}$$

$$\nabla v_l = 0 \tag{2}$$

where v_l is the blood flow velocity, p_l is the pressure, μ is the coefficient of dynamic viscosity of blood, and ρ is the density of blood. These equations can be transformed into the balance equations of a FE by using the Galerkin method. The incremental-iterative balance equation of a FE for a time step 'n' and equilibrium iteration 'i' has the form

$$\begin{bmatrix} \frac{1}{\Delta t}\mathbf{M} + {}^{n+1}\tilde{\mathbf{K}}_{vv}^{(i-1)} & \mathbf{K}_{vp} \\ \mathbf{K}_{vp}^{T} & \mathbf{0} \end{bmatrix} \begin{Bmatrix} \Delta\mathbf{V}^{(i)} \\ \Delta\mathbf{P}^{(i)} \end{Bmatrix}_{blood} = \begin{Bmatrix} {}^{n+1}\mathbf{F}_{ext}^{(i-1)} \\ 0 \end{Bmatrix} - \begin{bmatrix} \frac{1}{\Delta t}\mathbf{M} + {}^{n+1}\mathbf{K}^{(i-1)} & \mathbf{K}_{vp} \\ \mathbf{K}_{vp}^{T} & 0 \end{bmatrix} \begin{Bmatrix} {}^{n+1}\mathbf{V}^{(i-1)} \\ {}^{n+1}\mathbf{P}^{(i-1)} \end{Bmatrix} + \begin{Bmatrix} \frac{1}{\Delta t}\mathbf{M}\,{}^{n}\mathbf{V} \\ 0 \end{Bmatrix} \tag{3}$$

where ${}^{n+1}\mathbf{V}^{(i-1)}$ and ${}^{n+1}\mathbf{P}^{(i-1)}$ are the nodal vectors of blood velocity and pressure, with the increments in time step $\Delta\mathbf{V}^{(i)}$ and $\Delta\mathbf{P}^{(i)}$; Δt is the time step size and the left upper indices 'n' and 'n+1' denote start and end of the time step.

Using velocities as nodal variables, the incremental-iterative equations of the force-balance for a FE and per unit volume can be written in the usual form:

$$\left(\frac{1}{\Delta t}\mathbf{M} + \bar{\mathbf{K}}^{(i-1)}\right)\Delta\mathbf{V}^{(i)} = \mathbf{F}^{ext(i)} - \mathbf{F}^{\mathrm{int}(i-1)} - \frac{1}{\Delta t}\mathbf{M}\left(\mathbf{V}^{(i-1)} - \mathbf{V}^{t}\right) \tag{4}$$

where Δt is the time step, i is the iteration counter and $\mathbf{F}^{ext(i)}$ are external nodal forces acting on the element; $\mathbf{V}^{(i-1)}$ and $\mathbf{V}^{t}$ are nodal velocities at previous iteration and at the start of the time step, respectively. The mass and stiffness matrices are:

$$\mathbf{M} = \rho \mathbf{N}^T \mathbf{N}, \quad \bar{\mathbf{K}}^{(i-1)} = \left(\bar{\mathbf{B}}^T \mathbf{C}_T \bar{\mathbf{B}} \right)^{(i-1)} \tag{5}$$

where ρ is the mass density, and the vector of the internal nodal forces is:

$$\mathbf{F}^{\text{int}(i-1)} = \bar{\mathbf{B}}^{T(i-1)} \bar{\boldsymbol{\sigma}}^{(i-1)} \tag{6}$$

The tangent constitutive matrix $\mathbf{C}_T^{(i-1)}$ in the local system will be determined within the computational procedure.

There are two main approaches for finite element (FE) modeling of fluid-structure interaction (FSI) problems: (a) the strong coupling method, and (b) the loose coupling method. In the strong coupling approach, the solid and fluid domains are treated as a single mechanical system, with integrated modeling. Conversely, in the loose coupling method, the solid and fluid domains are modeled separately using different FE solvers—typically, the solid domain is simulated with a computational solid dynamics (CSD) solver, while the fluid domain uses a computational fluid dynamics (CFD) solver. Although these solutions are obtained independently, data such as parameters influencing both mediums are successively transferred between the solvers (Kojic et al., 2008; Filipovic et al., 2022a, 2022b).

At the boundary between fluid and solid, there is no slip, meaning that the nodes at this interface share the same displacements and velocities in both domains. In the strong coupling approach, the FE matrices and force terms for these shared nodes are combined during assembly, as is standard in FE procedures. In contrast, the loose coupling method formulates and solves the balance equations for each domain separately, avoiding some of the computational challenges associated with the strong coupling. Both methods are available in our PAK FE software package (Kojic et al., 2008). While similar results can be achieved with either approach, the loose coupling is generally preferred due to its lower computational demands. In this method, the equations are initially solved for the fluid domain. Once convergence is reached, the nodal forces for an element with boundary nodes are calculated as described in equation (6):

$$\mathbf{F}^E = \begin{bmatrix} \dfrac{1}{\Delta t}\mathbf{M} + \mathbf{K}_{vv} & \mathbf{K}_{vp} \end{bmatrix} \begin{Bmatrix} \mathbf{V} \\ \mathbf{P} \end{Bmatrix} \tag{7}$$

and the forces at the common boundary as the vector $\mathbf{F}^E$ are used.

2.4 Finite element (FE) solvers

This section explains how FE model was integrated with stretches along muscle fibers. Multi-scale model of muscle contraction together with graphical interpretation of the algorithm for the FSI problem is shown in Figure 1, (Kojic et al 2008).

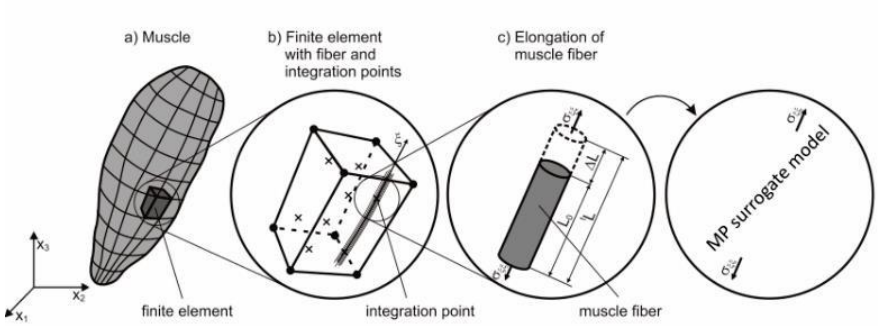

Fig. 2. Multi-scale model of muscle contraction. a) Muscle discretized into FEs, b) Muscle fiber within FE and integration points, c) local deformation of the muscle. Block-diagram of the solid-fluid interaction algorithm. Information and transfer of parameters between the CSD (computational solid dynamics) and CFD (computational fluid dynamics) solvers through the interface block (Kojic et al 2008).

Using input parameters, the current material state of the microscale model, and the applied stretch, the Mijailovich-Prodanovic (MP) surrogate model of sarcomere contractions (Mijailovich et al., 2021a, 2021b; Prodanovic et al., 2022) calculates the local active tension and instantaneous stiffness along the muscle fiber during each iteration (i), as illustrated in Figure 3. Subsequently, the macroscale model solves the equilibrium equation that incorporates these local active tension and stiffness values from the MP model, determining the stretch and total tension at the finite element (FE) integration points. This coupled, incremental, and iterative procedure continues until the changes in velocity and active tension between iterations fall below specified tolerances.

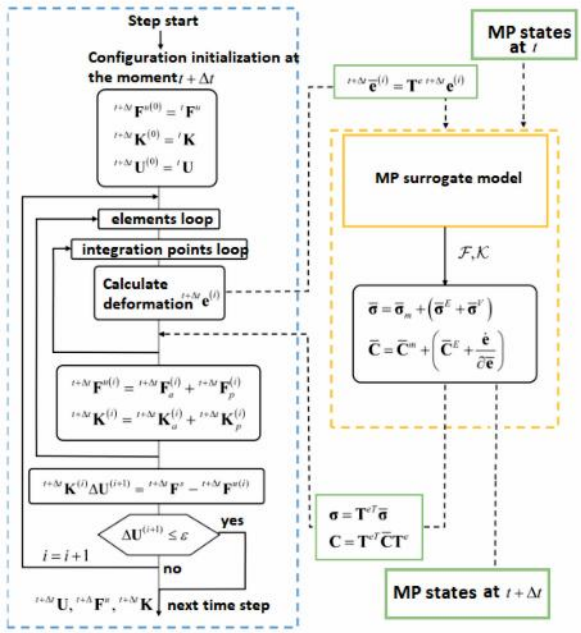

Fig. 3. Algorithm: FE analysis and MP surrogate model (Milicevic et al 2023, Filipovic et al 2022a, 2022b)

2.5. Drug testing workflow

Drugs used to treat various symptoms of cardiomyopathies target different mechanisms of action. In MUSICO simulations (Mijailovich et al., 2021a, 2021b), these drugs are categorized into three main groups or pathways, each characterized by their primary effect, such as modulating calcium transients or altering the kinetics of contractile proteins. Each of these groups is further divided into two subgroups, corresponding to the specific type of cardiomyopathy being treated.

2.5.1. Modulation of [Ca2+] transients

In this study, two types of drugs are utilized: for hypertrophic cardiomyopathy (HCM), Disopyramide, which reduces both the peak and baseline levels of [Ca2+] transients during twitch contractions; and for dilated cardiomyopathy (DCM), Digoxin, which increases the peak of [Ca2+] transients without affecting the timing to reach the peak or relaxation duration. The testing workflow for these drugs is illustrated in Fig. 3. The electrophysiological effects, including action potential alterations and ionic current changes, are simulated using the O'Hara-Rudy model, which generates intracellular calcium transients that serve as input for both the MUSICO and Mijailovich-Prodanovic (MP) surrogate models (Filipovic et al., 2022a, 2022b).

Fig. 4. The Pathway 1: Drug action via modulation of calcium transients through changes in ionic currents or membrane properties.

2.5.2 Changes in kinetic parameters

For hypertrophic cardiomyopathy (HCM), the drug Mavacamten influences the kinetics of the transition between disordered myosin detachment states and the ordered super-relaxed (SRX) state. In dilated cardiomyopathy (DCM), dATP modulates the rates of the cross-bridge cycle. The testing workflow for these drugs is illustrated in Fig. 5. Experimental in vitro data, which quantify the effects of specific drug doses, are used to estimate parameters for both the MUSICO and Mijailovich-Prodanovic (MP) surrogate models.

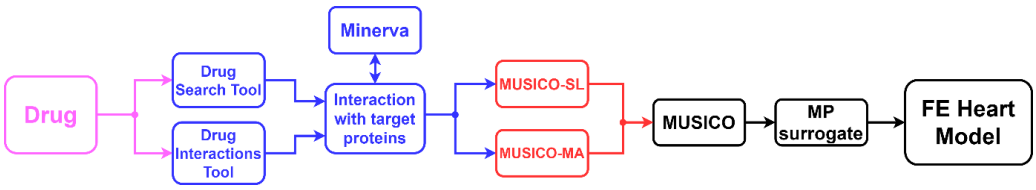

Fig. 5. The pathway 2: Drug action through changes in kinetics of contractile proteins.

Since drugs in groups I and II directly affect MUSICO and MP surrogate parameters, we were able to predict with our tools the outcome on force generation in sarcomeres during twitch contractions (Mijailovich et al 2021a).

2.5.3 Changes in macroscopic parameters

For hypertrophic cardiomyopathy (HCM), Entresto® influences the remodeling of the ventricular walls and modulates blood vessel elasticity, which generally decreases vascular resistance and enhances cardiac output. The workflow for testing these drugs is depicted in Fig.

6. Data from numerous clinical trials are used as inputs for finite element (FE) models to accurately simulate the specific effects of Entresto® (Filipovic et al., 2022a, 2022b).

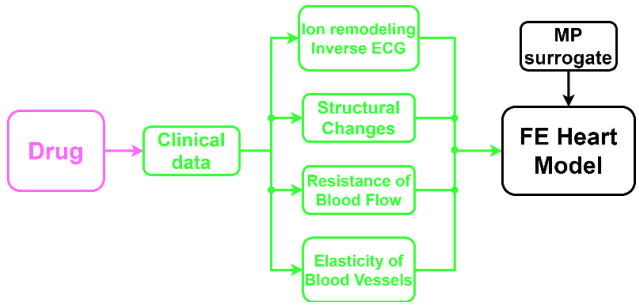

Fig. 6. The Pathway 3: Drug action through macroscopic structural and boundary condition changes.

3. Results and discussion

3.1. Results for electrical field

Here we present the electrical activity of the whole heart within the torso embedded environment, with spontaneous initiation of activation in the sinoatrial node and incorporating a specialized conduction system with heterogeneous action potential morphologies throughout the heart (Fig. 7).

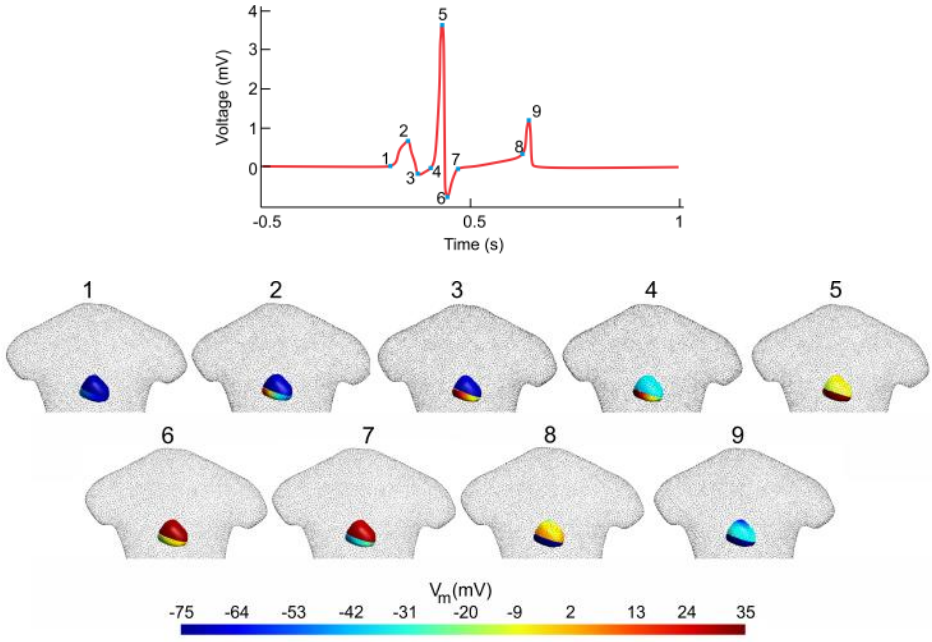

Fig. 7. Whole heart activation simulation from lead II ECG signal at various time points on the ECG signal. There are 1-9 activation sequences which are corresponding to ECG signal above. The color bar denotes mV of the transmembrane potential.

It illustrates the simulated and measured ECG for six electrodes (V1-V6) which are positioned on the chest to model the precordial leads for the normal heart volunteer. The normal ECG is in agreement with standard clinical findings (Filipovic et al 2022a, 2022b).

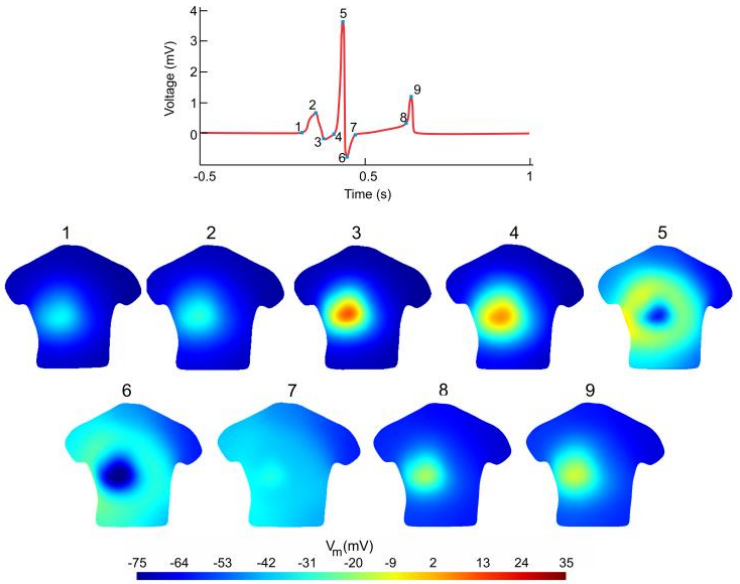

Fig 8. Body surface potential maps in a healthy subject during progression of ventricular activation in nine sequences which are corresponding to ECG signal above. The color bar denotes mV from heart activity range.

Body surface potential maps in the healthy subject during progression of ventricular activation in nine sequences which are corresponding to measured ECG signal are presented in Fig. 8 (Filipovic et al 2022a, 2022b).

3.2. PV diagram and blood flow through left ventricle

The following results are obtained with parametric model and describe how PV diagrams depend on the change of Ca2+, elasticity of the wall and the inlet and outlet velocity profile. This directly affects the ejection fraction. Basic geometry is shown in Figure 9, and standard inlet and outlet velocities are shown in Figure 10 (Filipovic et al 2022a, 2022b).

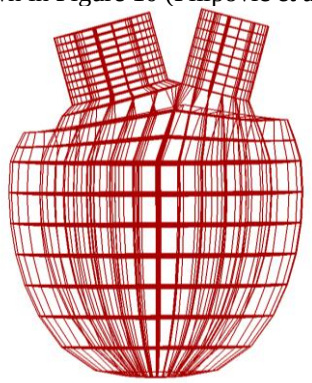

Fig. 9. Basic geometry of left ventricle parametric model

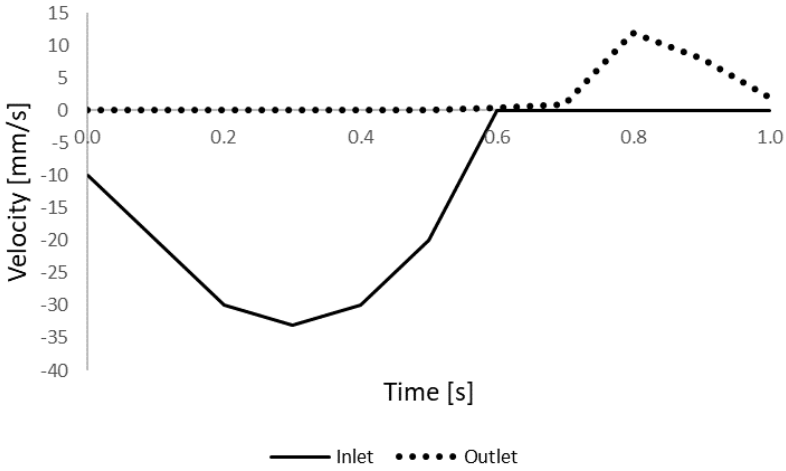

Fig. 10. Prescribed inlet and outlet velocities for aortic output and mitral input

Velocity field at 0.2s, 0.5s and 0.6s is shown in Figure **Fig**11. Pressure field at 0.2s, 0.5s and 0.6s is shown in Figure 12.

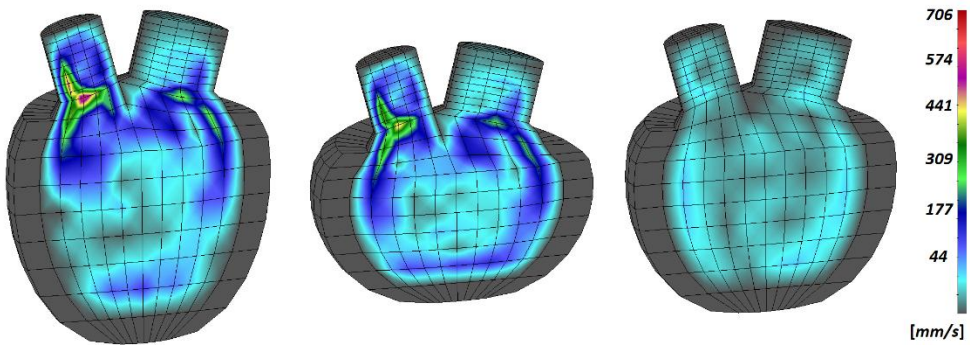

Fig. 11. Velocity field at 0.2s, 0.5s and 0.6s for parabolic Ca2+ concentration function

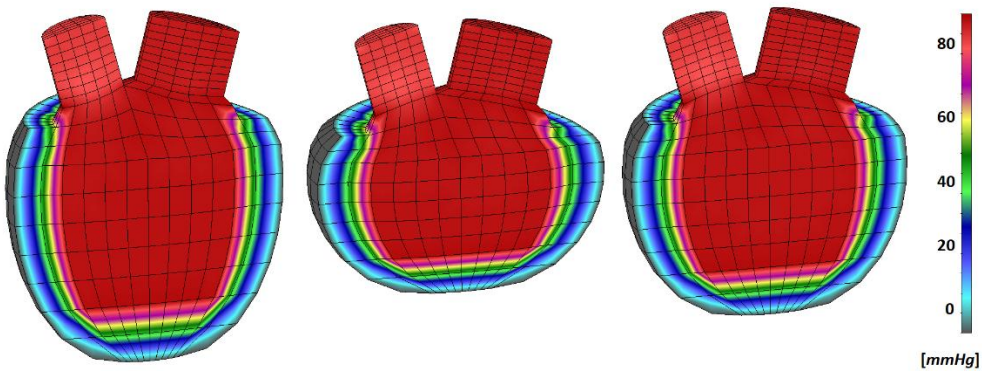

Fig. 12. Pressure field at 0.2s, 0.5s and 0.6s for parabolic Ca2+ concentration function

PV diagrams for 30% higher and 50% lower elasticity are shown in Figure 13 (Filipovic et al 2022a, 2022b).

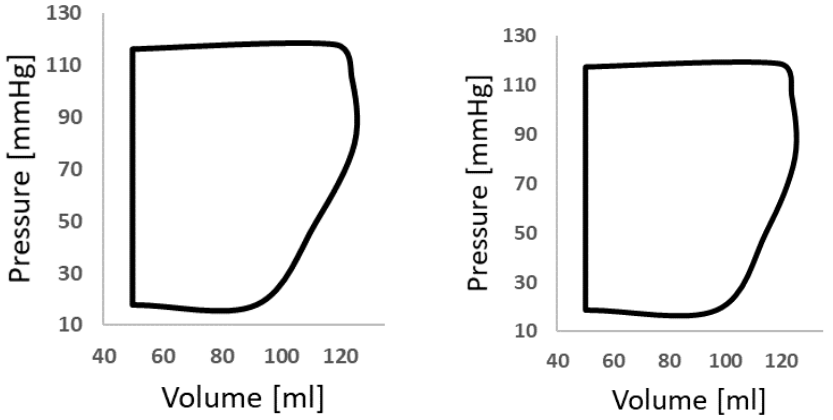

Fig. 13. PV diagrams for 20 % higher (left) and 20% lower (right) elasticity

3.3. Entresto drug influence

ENTRESTO® (Sacubitril/Valsartan) has been demonstrated to be more effective than enalapril in reducing the risk of death and hospitalization due to heart failure (HF). Several studies have also assessed the effects of sacubitril/valsartan on clinical, biochemical, and echocardiographic parameters in patients with heart failure with reduced ejection fraction (HFrEF). In this work, we simulated patient cases both before and after Entresto treatment. Prior to treatment, the pressure-volume (PV) diagram, along with diastolic and systolic pressure distributions, are shown in Fig. 14. These depict a typical hypertrophic cardiomyopathy patient with decreased ejection fraction and elevated systolic pressure (left in Fig. 14, pressure-volume diagram).

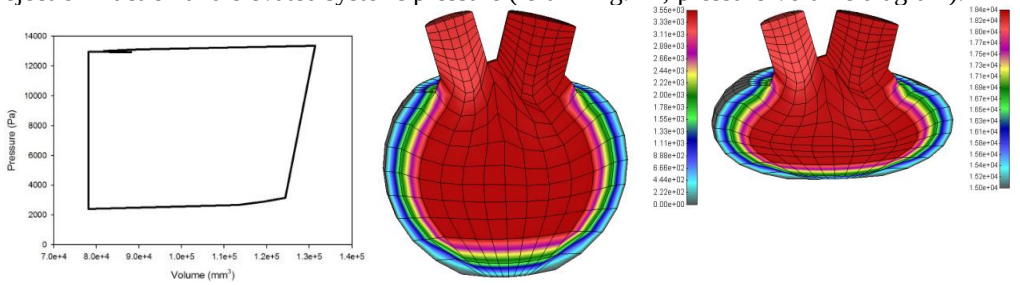

Fig. 14. PV diagram, pressure diastolic distribution, pressure systolic distribution for the case before Entresto treatment.

Following Entresto® treatment (Fig. 15), a reduction in systolic pressure is observed, along with an increased difference between end-diastolic and end-systolic volumes. This shift directly contributes to an improved ejection fraction. The pressure-volume diagram, as well as velocity distributions during diastolic and systolic phases after Entresto® treatment, are shown in Fig. 15 (Milicevic et al., 2023; Filipovic et al., 2022a, 2022b).

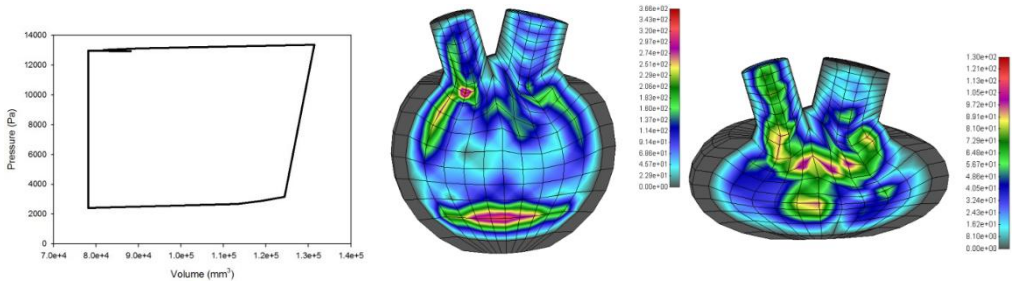

Fig. 15. PV diagram, velocity distribution in the diastolic phase, velocity distribution in the systolic phase for the case after Entresto treatment.

4. Conclusions

In the SILICOFCM project (2018), we developed an integrated heart modeling approach that incorporated simulated drugs for cardiomyopathy, emphasizing the electromechanical coupling of the left ventricle and the entire heart. The study classified drugs into three primary groups based on their main effects: (i) modulation of calcium transients, (ii) changes in contractile protein kinetics, and (iii) alterations in macroscopic structural properties or boundary conditions. The heart's geometry was represented with a model comprising seven regions: 1) sinoatrial node, 2) atria, 3) atrioventricular node, 4) His bundle, 5) bundle fibers, 6) Purkinje fibers, and 7) ventricular myocardium, utilizing a monodomain modified FitzHugh-Nagumo model of cardiac cells. To simulate the electrocardiogram (ECG), six electrodes (V1–V6) were positioned on the chest, and the results were compared with clinical data, optimizing heart potentials via an inverse ECG method.

The model captured the electrical activity of the whole heart within a torso-embedded environment, illustrating spontaneous activation originating from the sinoatrial node and a specialized conduction system displaying heterogeneous action potential morphologies. Body surface potential maps for healthy subjects demonstrated ventricular activation sequences that correlated with ECG signals across nine time points. Additionally, parametric analyses provided pressure-volume (PV) diagrams influenced by variations in calcium concentration, wall elasticity, and inlet/outlet velocities, which directly affected the ejection fraction (Filipovic et al., 2022a, 2022b).

Future work will focus on in silico clinical trials to compare body surface electrical activity with standard 12-lead ECG measurements. We also plan to investigate the mechanical effects of non-affine fiber kinematics in vascular and neural tissues, as well as electro-magneto-mechanical interactions within the nervous system, to enhance the multiscale fidelity and clinical applicability of our models. The study generated PV diagrams for various patient cases, including the effects of drugs like Entresto and Digoxin, demonstrating how these treatments influence cardiac function and ejection fraction through distinct PV shapes related to calcium concentrations.

Despite limitations—such as incomplete data on cardiac tissue properties and the difficulty of estimating subject-specific parameters from limited, noisy, non-invasive measurements—we advanced large-scale finite element simulations that can take several hours to compute. Nevertheless, tools like SILICOFCM (2018) and STRATIFYHF (2023) offer innovative platforms for assessing familial cardiomyopathy and heart failure risks, paving the way for future in silico clinical trials (Filipovic et al., 2022a, 2022b).

Acknowledgments: This study is supported by the European Union's Horizon 2020 research and innovation program under grant agreement SILICOFCM 777204, STRATIFYHF 101080905, and the Ministry of Education, Science and Technological Development of the Republic of Serbia through Contracts No. 451-03-9/2025-14/200378. This article reflects only the authors' view. The European Commission is not responsible for any use that may be made of the information the article contains.

References

Carney RM, Freedland KE (2009). Depression and heart rate variability in patients with coronary heart disease. *Cleve Clin J Med 2009*; 76(suppl 2):S13–S17

Filipovic N, Saveljic I, Sustersic, T Milosevic M, Milicevic B, Simic , Ivanovic M, Kojic M (2022a), *In Silico Clinical Trials for Cardiovascular Disease, J Vis Exp*, 2022 May 27;(183).doi: 10.3791/63573.

Filipovic N, Sustersic, T, Milosevic, M, Milicevic, B. Simic, V, Prodanovic, M, Mijailovic, S , Kojic M (2022b), SILICOFCM platform, multiscale modeling of left ventricle from echocardiographic images and drug influence for cardiomyopathy disease. *Comput. Methods Programs Biomed.* 227: 107194 (2022)

Fitzhugh, R. (1961), Impulses and physiological states in theoretical models of nerve membrane. *Biophysical J.*, 1: 445-466, 1961.

Gibbons Kroeker, C.A. Adeeb, S., Tyberg, J.V. and Shrive N.G. (2006), A 2D FE model of the heart demonstrates the role of the pericardium in ventricular deformation, *American Journal of Physiology*, vol. 291, no. 5, pp. H2229–H2236, 2006.

Guyton AC, Coleman TG, Cowley AW Jr, et al. (1972), Systems analysis of arterial pressure regulation and hypertension. *Ann Biomed Eng 1972*; 1:254–281

Holzapfel, GA., (2006) Determination of material models for arterial walls from uniaxial extension tests and histological structure. *Journal of Theoretical Biology*, Elsevier, 2006, 10.1016/j.jtbi.2005.05.006. hal-01299856

Katona PG, Poitras JW, Barnett GO, Terry BS. (1979), Cardiac vagal efferent activity and heart period in the carotid sinus refl ex. *Am J Physiol 1979*; 218:1030–1037

Kojic, M., Filipovic, N., Stojanovic, B., & Kojic, N. (2008). *Computer modeling in bioengineering: Theoretical Background, Examples and Software.* Chichester, England: John Wiley and Sons.

Kojic, M., Filipovic, N., Živkovic, M., Slavkovic, R., & Grujovic, N. (2008). PAK-FS Finite Element Program for Fluid-Structure interaction. Kragujevac, Serbia.

Kojic, M., Milosevic M, Simic V, Milicevic B, Geroski V, Nizzero S, Ziemys A, Filipovic N, Ferrari M, (2019), Smeared Multiscale Finite Element Models for Mass Transport and Electrophysiology Coupled to Muscle Mechanics, *Frontiers in Bioengineering and Biotechnology*, ISSN 2296-4185, Vol. 7, 381, pp. 1-16, 2296-4185, 2019.

Lauer MS (2009). Autonomic function and prognosis. *Cleve Clin J Med 2009*; 76(suppl 2):S18–S22.

Mijailovich, S.M.; Prodanovic, M., Poggesi, C.; Geeves, M.A.; Regnier, M. (2021a) Multiscale Modeling of Twitch Contractions in Cardiac Trabeculae. *J. Gen. Physiol.* 2021, *153*, doi:10.1085/jgp.202012604.

Mijailovich, S.M.; Prodanovic, M.; Poggesi, C.; Powers, J.D.; Davis, J.; Geeves, M.A.; Regnier, M. (2021b) The Effect of Variable Troponin C Mutation Thin Filament Incorporation on Cardiac Muscle Twitch Contractions. *J. Mol. Cell. Cardiol.* 2021, *155*, 112–124, doi:10.1016/j.yjmcc.2021.02.009.

Milicevic B, Milosevic M, Simic V, Trifunovic D, Stankovic G, Filipovic N, Kojic M, (2023), Cardiac hypertrophy simulations using parametric and echocardiography-based left ventricle

model with shell finite elements. *Comput. Biol. Medicine 157*: 106742 (2023)

MUSICO software (2023), https://www.solindies.com/musico

Nagumo, J., Arimoto S, Yoshizawa S, (1962), An active pulse transmission line simulating nerve axon. *Proc. IRE.*, 50: 2061-2070, 1962.

Piccirillo G et al. (2009) Autonomic nervous system activity measured directly and QT interval variability in normal and pacing-induced tachycardia heart failure dogs. *J. Am. Coll. Cardio* 54, 840–850. (doi:10.1016/j.jacc.2009.06.008)

Prodanovic, M.; Geeves, M.A.; Poggesi, C.; Regnier, M.; Mijailovich, S.M. (2022) Effect of Myosin Isoforms on Cardiac Muscle Twitch of Mice, Rats and Humans. *Int. J. Mol. Sci.* 2022, *23*, 1135, doi:10.3390/ijms23031135.

Pullan, A.J. Buist, M.L. and Cheng L.K. (2005), Mathematically Modelling the Electrical Activity of the Heart—From Cell To Body Surface and Back Again,*World Scientific*, 2005.

Rashba EJ, Cooklin M, MacMurdy K, Kavesh N, Kirk M, Sarang S, Peters RW, Shorofsky SR, Gold MR. (2002) Effects of selective autonomic blockade on T-wave alternans in humans Circulation 105, 837–842. (doi:10.1161/hc0702.104127)

SILICOFCM project (2018-2023), In Silico trials for drug tracing the effects of sarcomeric protein mutations leading to familial cardiomyopathym, *EU Horizon 2020*, No 777204, www.silicofcm.eu

Sovilj, S., Magjarević R, Lovell N, Dokos S, (2013) A simplified 3D model of whole heart electrical activity and 12-lead ECG generation. *Computational and Mathematical Methods in Medicine*, doi:10.1155/2013/134208, 2013.

STRATIFYHF project (2023-2028), Artificial intelligence-based decision support system for risk stratification and early detection of heart failure in primary and secondary care, *European Union's Horizon Europe research and innovation programme under grant agreement No 101080905*, https://stratifyhf.eu/

Trudel, M.C., Dub´e, B, Potse, M., Gulrajani RM, and Leon LJ (2004), Simulation of QRST integral maps with a membrane based computer heart model employing parallel processing, *IEEE Transactions on Biomedical Engineering*, vol. 51, no. 8, pp. 1319–1329, 2004.

Van Oosterom A (1999), The use of the spatial covariance in computing pericardial potentials. *IEEE Transactions on biomedical engineering 46*, 7, 778–787, 1999.

Van Oosterom A (2001), The spatial covariance used in computing the pericardial potential distribution. *Computational Inverse Problems in Electrocardiography*, 1–50, 2001

Van Oosterom A (2003), Source models in inverse electrocardiography. Int J Bioelectromagn 5 211–214, 2003.

Van Oosterom A (2010), The equivalent double layer: source models for repolarization. *In Comprehensive Electrocardiology*. Springer, pp. 227–246., 2010.

Wang, Y and Rudy Y (2006), Application of the method of fundamental solutions to potential-based inverse electrocardiography. *Annals of biomedical engineering* 34, 8, 1272–1288, 2006.

Wilhelms M., Dossel O., Seemann G. (2011), In silico investigation of electrically silent acute cardiac ischemia in the human ventricles. *IEEE Trans Biomed Eng 58*, 2961–4, 2011.